

Primordial power spectrum from WMAP

Arman Shafieloo and Tarun Souradeep
*Inter-University Centre for Astronomy and Astrophysics,
 Post Bag 4, Ganeshkhind, Pune 411 007, India.*

The observed angular power spectrum of the cosmic microwave background temperature anisotropy, C_l , is a convolution of a cosmological radiative transport kernel with an assumed primordial power spectrum of inhomogeneities. Exquisite measurements of C_l over a wide range of multipoles from the Wilkinson Microwave Anisotropy Probe (WMAP) has opened up the possibility to deconvolve the primordial power spectrum for a given set of cosmological parameters (base model). We implement an improved (error sensitive) Richardson-Lucy deconvolution algorithm on the measured angular power spectrum from WMAP assuming the concordance cosmological model. The most prominent feature of the recovered $P(k)$ is a sharp, infra-red cut off on the horizon scale. The resultant C_l spectrum using the recovered spectrum has a likelihood far better than a scale invariant, or, 'best fit' scale free spectra ($\ln L = 25$ w.r.t. Harrison Zeldovich, and, $\ln L = 11$ w.r.t. power law with $n_s = 0.95$). The recovered $P(k)$ has a localized excess just above the cut-off which leads to great improvement of likelihood over the simple monotonic forms of model infra-red cut-off spectra considered in the post WMAP literature. The recovered $P(k)$, in particular, the form of infra-red cut-off is robust to small changes in the cosmological parameters. We show that remarkably similar form of infra-red cutoff is known to arise in very reasonable extensions and refinements of the predictions from simple inflationary scenarios. Our method can be extended to other cosmological observations such as the measured matter power spectrum and, in particular, the much awaited polarization spectrum from WMAP.

PACS numbers: 98.80.Es, 98.70.Vc

I. INTRODUCTION

Increasingly accurate measurements of the anisotropy in the temperature of the cosmic microwave background (CMB) has ushered in an era of precision cosmology. A golden decade of CMB anisotropy measurements by numerous experiments was topped by the results from the first year of data obtained by the Wilkinson Microwave Anisotropy Probe (WMAP) [1]. Under simple hypotheses for the spectrum of primordial perturbations, exquisite estimates of the cosmological parameters have been obtained from the angular power spectrum measurement by WMAP combined with other cosmological observations [2]. Although the assumed, scale free (with mild deviations), initial power spectra may be a generic prediction of the simplest scenarios of generation of perturbations during inflation, initial spectra with radical deviations are known to arise from very reasonable extensions, or, refinements to the simplest scenarios [3, 4, 5]. Consequently, cosmological parameter estimation from the CMB anisotropy and the matter power spectrum obtained from redshift surveys, weak gravitational lensing and Ly- α absorption, depends sensitively on the dimensionality, nature and freedom in the parameter space of initial conditions [6].

The angular power spectrum, C_l , is a convolution of the initial power spectrum $P(k)$ generated in the early universe with a radiative transport kernel, $G(l, k)$, that is determined by the current values of the cosmological parameters. The remarkably precise observations of the angular power spectrum C_l by WMAP, and the concordance of cosmological parameters measured from different cosmological observations opens up the avenue to directly recover the initial power spectrum of the density perturbation from the observations. The Richardson-Lucy (RL) method deconvolution was shown to be a promising and powerful method to measure the power spectrum of initial perturbations from the CMB angular power spectrum [7]. In this paper, we apply the method to the CMB anisotropy spectrum measured by WMAP. We have also devised and implemented an improvement to the RL scheme, whereby the iterative deconvolution algorithm is designed to converge and *match the measurements only within the given error-bars*.

The direct numerical deconvolution has clear advantages over the other prevalent approach of obtaining the most likely parameter values for a parametric model primordial spectra [52]. First, as emerges from our work, the direct method can reveal features that are not anticipated by the parametric model spectra, hence would be completely missed out in the latter approach. Second, in the absence of an accepted early universe scenario (more narrowly, a favored model of inflation), it is difficult to *a priori* set up and justify the chosen space of initial conditions. The complex covariances

between the cosmological and the initial parameters are sensitive to the parameterization of the space of initial spectra adopted. Efforts along these lines are further obscured by issues such as the applicability of the Occam's razor to dissuade extension of the parameter space of initial conditions. Such deliberations have been recently framed in the more quantitative language of Bayesian evidence to evaluate and select between possible parameterizations [13]. However, this approach cannot really point to a preferred parameterization. Whereas, in the direct approach we can evade the issue of appropriate parameterization of the initial power spectrum. For a given set of cosmological parameters, our method obtains the primordial power spectrum that ‘maximizes’ the likelihood. Hence, the space of parameters remains that of the (more widely accepted and agreed up on) cosmological parameters alone. In principle, it is possible to explore the entire space of cosmological parameters along the lines being done routinely, and instead of simply computing the likelihood for a given model initial power spectrum, one obtains the initial power spectrum that maximizes the likelihood at that point and assigns that likelihood to that point in the space of cosmological parameters [53]. However, in this paper we limit ourselves to obtaining the primordial spectrum for a few given sets of ‘best fit’ cosmological parameters and showing that recovered $\mathcal{P}(\mathbf{k})$ is robust to small local variations in the cosmological parameters. We defer the wide exploration of the cosmological parameter space to future work.

In section II, we describe the problem and present the deconvolution method, details of its implementation and tests of recovering known primordial spectra from synthetic angular power spectrum data. The recovered spectrum from WMAP data using our method is described in section III. The recovered primordial spectrum has statistically significant features that are robust to the variations in the cosmological parameters. In section IV, the recovered spectrum is shown to be tantalizingly similar to some forms of broken scale invariant spectra known to arise from reasonable variations of the simplest inflationary scenario.

II. METHOD

A. Integral equation for CMB anisotropy

In this subsection we recall the integral equation for the angular power spectrum of CMB anisotropy and set up the inverse problem that we solve using a deconvolution method. The observed CMB anisotropy $\Delta_T(\mathbf{n})$ is one realization of a random field on the surface of a sphere and can be expressed in terms of the random variates $a_{\mathbf{l}m}$ that are the coefficients of a Spherical Harmonic expansion given by

$$\Delta_T(\mathbf{n}) = \sum_{l=2}^{\infty} \sum_{m=-l}^{l} a_{lm} Y_{lm}(\mathbf{n}) \quad (2.1)$$

where $Y_{lm}(\mathbf{n})$ are the Spherical Harmonic functions. For an underlying isotropic, Gaussian statistics, the angular power spectrum, C_l defined through

$$\langle a_{lm} a_{l'm'}^* \rangle = C_l \delta_{ll'} \delta_{mm'} \quad (2.2)$$

completely characterizes the CMB anisotropy.

In a flat universe the temperature fluctuation in the CMB photons at the location \mathbf{x} at the present conformal time η_0 propagating in a direction \mathbf{n} is

$$\Delta_T(\mathbf{x}; \mathbf{n}; \eta_0) = \int_0^{\eta_0} d^3k e^{i\mathbf{k} \cdot \mathbf{x}} (\mathbf{k}; \mathbf{n}; \eta_0) \quad (2.3)$$

For globally isotropic cosmology, the temperature fluctuation $(\mathbf{k}; \mathbf{n}; \eta_0) = (\mathbf{k} - \mathbf{n}; \eta_0)$ can be expanded in terms of Legendre polynomials leading to

$$\Delta_T(\mathbf{x}; \mathbf{n}; \eta_0) = \int_0^{\eta_0} d^3k e^{i\mathbf{k} \cdot \mathbf{x}} \sum_{l=0}^{\infty} (-i)^l (2l+1) P_l(\hat{\mathbf{k}} \cdot \mathbf{n}) P_l(\hat{\mathbf{k}} \cdot \mathbf{n}) \quad (2.4)$$

The angular power spectrum C_l given by the coefficients of Legendre expansion is then expressed as

$$C_l = (4\pi)^{-2} \int_0^\infty \frac{dk}{k} P(k) j_{l+1/2}(k; 0)^2 \quad (2.5)$$

where $P(k)$, the power spectrum of the *primordial (scalar) metric* initial perturbation δ_{prim} , is given by

$$\langle \delta_{\text{prim}}(k) \delta_{\text{prim}}^*(k') \rangle = \frac{P(k)}{k^3} \delta(k - k') \quad (2.6)$$

because the k space modes are uncorrelated in a homogeneous space. The spectrum $P(k)$ represents the *r.m.s.* power in the scalar metric perturbations per logarithmic interval dk/k at a wavenumber k . It is related to power spectrum of the primordial modes of density perturbations, δ_k , as $P(k) = \langle \delta_k \delta_k^* \rangle k^3$. For the conventional scale free parameterization, the spectral index n_s is defined through $\langle \delta_k \delta_k^* \rangle = A k^{n_s}$. *The power spectrum $P(k)$ is a constant for the scale invariant Harrison-Zeldovich spectrum (corresponds to $n_s = 1$).*

The harmonics of the temperature fluctuations at the current epoch, $\delta_{Tl}(k; 0)$, is obtained from the solution to the Boltzmann equation for the CMB photon distribution. In this paper we use $\delta_{Tl}(k; 0)$ computed by the CMBfast software [14]. Numerically, a suitably discretized space of wave-numbers, k_i is used where the following discrete version of integral eq. (2.5) is applicable

$$C_l = \sum_i G(l; k_i) P(k_i) \quad (2.7)$$

$$G(l; k_i) = \frac{k_i}{k_i^3} j_{l+1/2}(k_i; 0)^2 :$$

In the above equation, the ‘*target*’ angular power spectrum, $C_l = C_l^D$, is the data given by observations, and the radiative transport kernel, $G(l; k)$ is fixed by the cosmological parameters of the ‘*base*’ model. (The kernel $G(l; k)$ also includes the effect of geometrical projection from the three dimensional wavenumber, k , to the harmonic multipole, l on the two dimensional sphere.) For a given $G(l; k)$, obtaining the primordial power spectrum, $P(k)$ from the measured C_l is clearly a deconvolution problem. An important feature of our problem is that C_l^D , $G(l; k)$ and $P(k)$ are all positive definite. However, to get reliable results from the deconvolution, we require high signal to noise measurements of C_l^D over a large range of multipoles with good resolution in multipole, preferably, from a single experiment to avoid the uncertainties of relative calibration [54].

Ideally, it will be best to measure each C_l^D independently. In practice, incomplete sky coverage and other effects limit the resolution in multipole space. All experiments provide band power estimates, $C_b(l_b) = \sum_l W_l^{(b)} C_l$ which are averaged linear combinations of the underlying C_l . Since eq. (2.7) is linear, a similar equation holds for all the band powers with a kernel, $G(l_b; k_i) = \sum_l W_l^{(b)} G(l; k_i)$. *For simplicity and brevity of notation, we retain the notation C_l^D and $G(l; k)$ for band power estimates with l denoting the bin center. We also implicitly assume a discrete wavenumber k instead of carrying the clumsy notation, k_i .*

As mentioned in more detail in section III A, the CMB angular power spectrum from WMAP ranges from the quadrupole, $l = 2$ to 900. Moreover, the ‘full sky’ coverage of WMAP implies good resolution in multipole space. We use WMAP TT (temperature-temperature) binned power spectrum as C_l^D in eq. (2.7). We use CMBfast software to compute the $G(l; k)$ matrix for the post-WMAP ‘best fit’ cosmological parameters. We emphasize that although the $P(k)$ is recovered using binned data, the significance (performance) of the recovered spectrum is evaluated using the WMAP likelihood of entire unbinned C_l properly accounting for covariances. The likelihood is computed using the numerical code, data and its error covariance provided by the WMAP collaboration with the release of the first year data.

In this work we limit our attention to the angular spectrum of the temperature anisotropy, C_l^{TT} . Including the polarization of CMB photons, equations similar to eq. (2.5) can be also written for the three additional angular power spectra, C_l^{TE} , C_l^{EE} and C_l^{BB} involving their corresponding

kernels. It will certainly be interesting to include these when more complete polarization data is available in the future. At present, only the $C_1^{\text{T E}}$ spectrum has been published by the WMAP team which is not positive definite and hence, not ideally suited for our method. However, once $C_1^{\text{E E}}$ data is made available, our method can readily accommodate both $C_1^{\text{T E}}$ and $C_1^{\text{E E}}$ together since combinations such as $C_1^{\text{T T}} - 2C_1^{\text{T E}} + C_1^{\text{E E}}$ are positive definite.

B. Deconvolution method

The Richardson-Lucy (RL) algorithm was developed and is widely used in the context of image reconstruction in astronomy [16, 17]. However, the method has also been successfully used in cosmology, to deproject the 3-D correlation function and power spectrum from the measured 2-D angular correlation and 2-D power spectrum [18, 19]. We employ an improved RL method to solve the inverse problem for $P(k)$ in eq. (2.7). The advantage of RL method is that positivity of the recovered $P(k)$ is automatically ensured, given $G(l;k)$ is positive definite and C_1 's are positive.

The RL method is readily derived from elementary probability theory on distributions [16]. To make this connection, we consider normalized quantities [55]

$$\sum_l C_1 = 1; \quad \sum_k P(k) = 1; \quad \sum_l G(l;k) = 1; \quad (2.8)$$

This allows us to view the functions, $P(k)$ and C_1 as one dimensional distributions, and $G(l;k)$ as a conditional probability distribution. Further, for convenience (not necessity) of writing an infinitesimal measure dl we view l to be continuous. The integrand in the integral eq. (2.5) suggests defining two other probability distributions $Q(l;k)$ and $L(k;l)$, such that

$$G(l;k) P(k) dl dk = Q(l;k) dl dk = L(k;l) C_1 dl dk \quad (2.9)$$

Dividing the both side of eq. (2.9) by $C_1 dl dk$ we obtain

$$L(k;l) = \frac{P(k)}{C_1} G(l;k); \quad (2.10)$$

The normalization conditions imply

$$P(k) = \int_l Q(l;k) dl = \int_l C_1 L(k;l) dl; \quad (2.11)$$

which in the discrete l space reads

$$P(k) = \sum_l Q(l;k) = \sum_l L(k;l) C_1; \quad (2.12)$$

The RL method iteratively solves the eqs. (2.10) and (2.12). Starting from an initial guess $P^{(0)}(k)$, L is obtained using eq. (2.10) as the first step. The second step is to obtain a revised $P^{(1)}(k)$ using eq. (2.12). These two steps are repeated iteratively with the $P^{(i)}(k)$ obtained after iteration i feeding into the iteration $i+1$. In principle, the final answer could depend on the initial guess but in practice, for a large variety of problems, RL is known leads to the correct answer even a crude estimation of the initial guess. In particular, for our problem the RL rapidly converges to the same solution $P(k)$ independent of the initial guess $P^{(0)}(k)$. This is demonstrated in Appendix A 1.

The iterative method can be neatly encoded into a simple recurrence relation. The power spectrum $P^{(i+1)}(k)$ recovered after iteration $(i+1)$ is given by

$$P^{(i+1)}(k) = P^{(i)}(k) \sum_l G(l;k) \frac{C_1^{\text{D}} C_1^{(i)}}{C_1^{(i)}} \quad (2.13)$$

where C_1^D is the measured data (target) and $C_1^{(i)}$ is the angular power spectrum at i^{th} iteration obtained from eq. (2.7) using the recovered power spectrum $P^{(i)}(k)$. Eq. (2.13) with eq. (2.7) for obtaining $C_1^{(i)}$ from $P^{(i)}(k)$ completely summarizes the standard RL method.

Due to noise and sample variance, the data C_1^D is measured within some non-zero error bars δ_1 . The standard RL method does not incorporate the error information at all. Consequently, a well known drawback of the standard RL method is that at large iterations the method starts fitting features from the noise. Modified forms of RL that address this issue have been proposed (e.g., see damped RL method in [20]). In our problem, this problem manifests itself as very non-smooth deconvolved spectrum $P(k)$ that has poor likelihood with the full WMAP spectrum data. We devise a novel method to make the RL method sensitive to the error δ_1 by modifying eq. (2.13) to

$$P^{(i+1)}(k) = P^{(i)}(k) + \frac{G(l; k)}{C_1^{(i)}} \frac{C_1^D - C_1^{(i)}}{C_1^{(i)}} \tanh^2 \left(\frac{(C_1^D - C_1^{(i)})^2}{\delta_1^2} \right)^{\frac{1}{2}} : \quad (2.14)$$

The idea is to employ a ‘convergence’ function to progressively weigh down the contribution to the correction $P^{(i+1)} - P^{(i)}$ from a multipole bin where $C_1^{(i)}$ is close C_1^D within the error bar δ_1 . This innovation significantly improves the WMAP likelihood of the deconvolved spectrum. For certain $G(l; k)$, the improvement is so dramatic that using IRL becomes very crucial to successful recovery of the spectrum (see III C). The final results are not sensitive to the exact functional form of the convergence function. The choice given in eq. (2.14) works well but is not unique in any sense.

At every iteration of the IRL scheme, we compute the χ^2 of the $C_1^{(i)}$ with respect to the binned data C_1^D . We have found that the IRL iterations (as well as the RL) march almost monotonically toward improved (smaller) χ^2 . We halt the iterations when the χ^2 does not change appreciably in subsequent iterations of IRL.

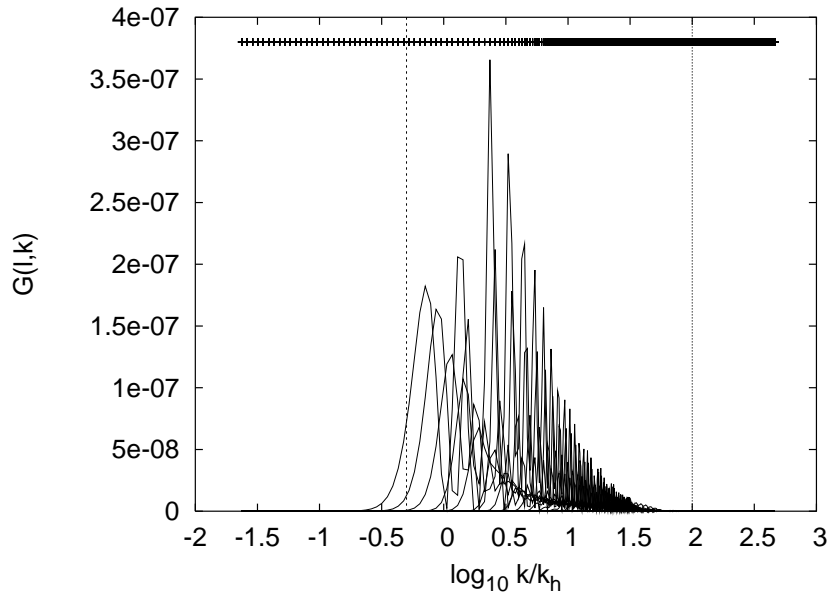


FIG. 1: The curves are $G(l; k)$ versus wavenumber k used in our work. $G(l; k)$ is averaged over $G(l; k)$ within multipole bins used by WMAP. The two vertical lines roughly enclose the region of k -space strongly probed by the kernel where the primordial spectrum can be expected to be recovered reliably. The k -space sampling used is indicated by the line of ‘+’ symbols at the top of the plot.

C. Post processing the deconvolved spectrum

The deconvolution algorithm produces a ‘raw’ $P(k)$ that has to be processed further. The raw deconvolved spectrum has spurious oscillations and features arising largely out of the k space

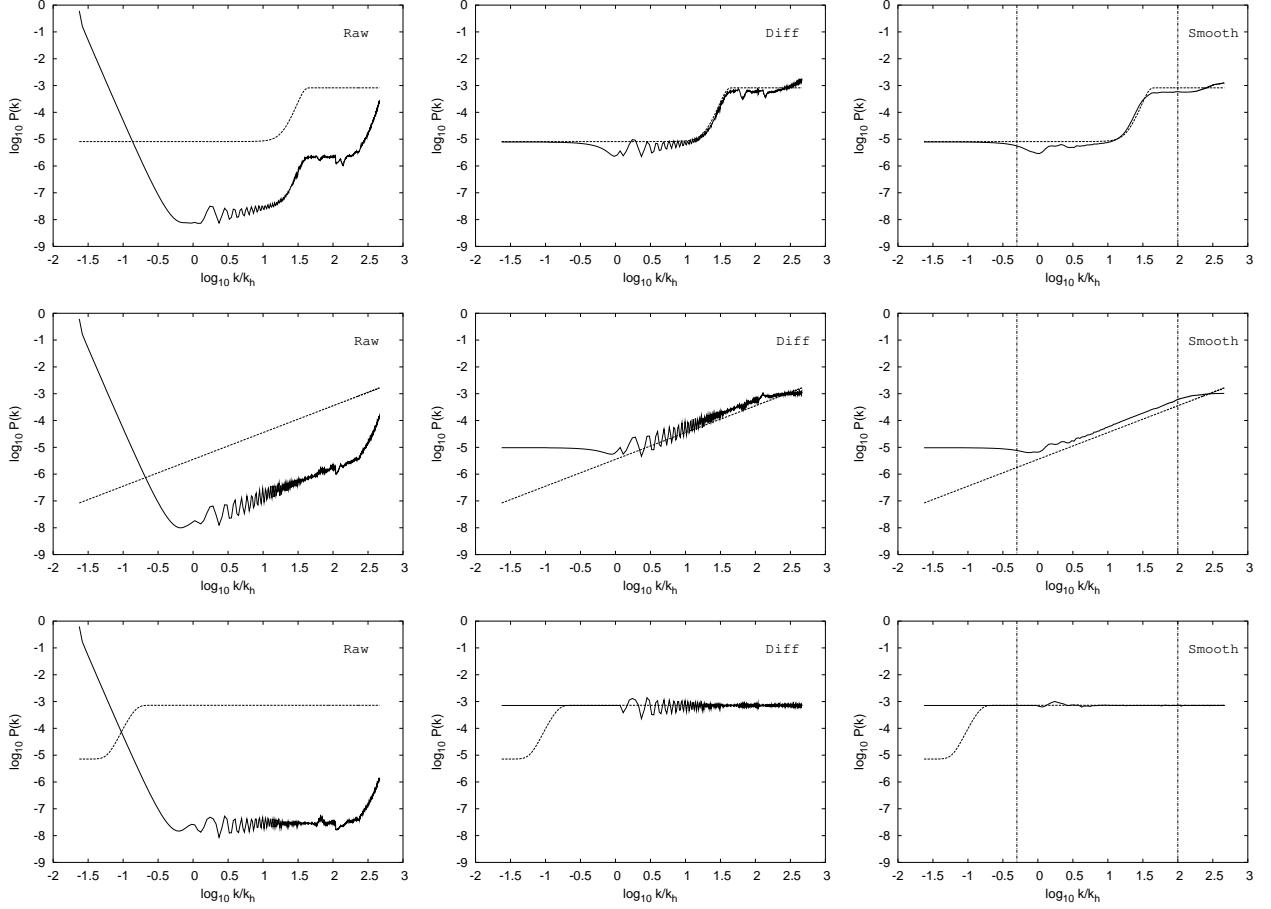


FIG. 2: Each of the three rows in the panel of figures illustrates the recovery the primordial power for a test case using C_1 arising from a known non-scale invariant primordial spectrum. The first column compares the raw deconvolved spectrum with the input spectrum. Note the similar artifacts in the all the raw spectra at the low and high k end discussed in the text. The feature is outside the range of $G(\mathbf{l}; \mathbf{k})$ and is completely missed in the third case. The second, column is the differenced spectrum obtained by dividing out by a raw reference spectrum. The differenced spectrum resembles the input spectrum (top two cases) with small oscillations. The third column shows that the final recovered spectrum obtained by smoothing the differenced spectrum matched the input spectrum very well.

sampling and binning in \mathbf{l} -space. These numerical artifacts are common to all recovered spectra recovered with same $G(\mathbf{l}; \mathbf{k})$. Fig. 1 shows the plot of the binned kernel $G(\mathbf{l}; \mathbf{k})$ for the \mathbf{l} -space bins used by WMAP [21, 22]. The wavenumbers are scaled by horizon scale, $k_h = 2\pi / \theta_{rec} = 0.0026$. The sampling of k space used here is also indicated in the figure. We find that removing these artifacts and smoothing the resultant spectrum improves the WMAP likelihood of the corresponding C_1 .

We illustrate the steps of removing the numerical artefacts and smoothing with test case examples of synthetic C_1 from known test primordial spectrum. The first column of Fig. 2 shows the ‘raw’ spectrum obtained. A comparison with the known spectra shows similar numerical noise and artefacts in all the cases, especially, the rise at very low and very high wave numbers. As shown in appendix A3, the main artifacts at the low and high k ends can be understood and modeled analytically. However we find it easier to remove them constructing a numerically generated template reference spectrum that also takes care of small features which appear due to changes in the k spacing. To remove these numerical artifacts, we generate a synthetic C_1 using a Harrison-Zeldovich spectrum and then apply the deconvolution method to recover a ‘reference’ spectrum $P_{ref}(\mathbf{k})$. We divide every ‘raw’ spectrum by $P_{ref}(\mathbf{k})$ to obtain a ‘differenced’ spectrum that does not have numerical artifacts as seen in middle column (“diff.”) of Fig 2.

The difference spectra are a noisy version of the test spectra. Hence, the exercise with the test spectra suggests that the differenced spectrum needs to be ‘suitably’ smoothed to recover the true power spectrum. A simple smoothing procedure with simple fixed width window function leads to a satisfactory recovery of the test spectrum. (A ‘Bowler hat’ window constructed with hyperbolic tangent functions is used for smoothing.)

The last column in Fig 2 shows the remarkably successful recovery of the test spectra in the top two case. As expected, the $P(k)$ is recovered best in the k space (within the vertical lines in bottom row of Fig 2) where the kernel $G(l;k)$ is significant (marked by the vertical lines in Fig. 1 and 2). In the bottom row, the feature in the test spectrum is outside the range of the kernel $G(l;k)$, and, as expected, the recovery process misses it completely. For the top row, if we ignore the region where there is no power for $G(l;k)$ the recovered spectrum is well matched with the test spectrum. The match may be further improved by using more elaborate, adaptive smoothing procedure.

For application to real data, the phrase ‘suitable smoothing procedure’ may appear ambiguous. But the smoothing is in fact very well defined for real data by demanding that the smoothed $P(k)$ produces a theoretical C_1 that has higher likelihood given the data. We find that this approach works extremely well. The deconvolution algorithm uses the binned C_1 data, hence the theoretical C_1 corresponding to the recovered $P(k)$ fits the binned data very well. However, the WMAP likelihood of the theoretical C_1 suffers owing to spurious oscillations in the differenced spectra. The WMAP likelihood improves as the differenced spectra, $P_{di}(k)$ is smoothed. We smooth the differenced spectrum so that WMAP likelihood of the corresponding theoretical C_1 is maximized. Although it is difficult to establish that the final result is the unique solution with maximum likelihood, in practice, our simple scheme does lead to a well defined result (no distinct degenerate solutions were found). Since our smoothing procedure is simple minded, possible avenues for improvement with more elaborate smoothing procedure remain open. Work is in progress to employ wavelet decomposition for the smoothing procedure.

III. APPLICATION TO THE WMAP CMB ANISOTROPY SPECTRUM

We apply the method described in the previous section to the angular power spectrum obtained with the first year of WMAP data publicly released in February 2003 [1] to recover the primordial power spectrum. In section III A, the publicly available WMAP data and how it is used in our work is discussed. We also describe the choice of the ‘base’ cosmological model. The recovered primordial power spectrum for this model is presented in section III B. The next section III C presents the effect of varying the cosmological parameters (within 1σ error bars) on the recovered primordial power spectrum. We also present the primordial spectrum for a set of cosmological models with large optical depths ($\tau = 0.17; 0.25$) corresponding to possible the early reionization scenarios suggested by the WMAP temperature-polarization (TE) cross-spectrum.

A. WMAP anisotropy data and the cosmological model

Accurate measurements of the angular power spectrum of CMB anisotropy was derived from the first year WMAP data recently [21]. The spectrum obtained by averaging over 28 cross-channel power measurements is essentially independent of the noise properties of individual radiometers. The power at each multipole ranging from $l = 20$ to 900 was estimated together with the covariance [56]. The instrumental errors are smaller than the cosmic variance up to $l = 350$, and the signal to noise per mode is above unity up to $l = 650$.

The angular power spectrum estimate and covariance matrix are publicly available at the LAMBDA data archive [57]. The WMAP team has also made available a suite of F90 codes that computes the likelihood for a given theoretical C_1 spectrum given the full angular power spectrum included the covariance measured by WMAP. We use the TT likelihood code for computing the likelihood of C_1 obtained from the recovered power spectrum and refer to these numbers as the ‘WMAP likelihood’ in the paper.

In addition, the WMAP team has also obtained a binned angular power spectrum where an average C_1 is defined over bins in multipole space. The binned C_1 estimates can be treated as independent data points since the covariance between binned estimates is negligible. We use this

binned spectrum as C_1^D in the deconvolution of eq. (2.7). (We are aware of but do not consider the revised estimates of the low multipoles made by other authors after the WMAP results [23, 24])

The variance of C_1 measurements is given by

$$\sigma_1^2 = \frac{2}{(2l+1)f_{\text{sky}}} C_1^T + \frac{2}{N} \frac{\sigma_p^2}{B_1^2} ; \quad (3.1)$$

where σ_N is the noise per pixel, σ_p the angular pixel size, f_{sky} is the fraction of sky covered and B_1 is the transform of the experimental beam [25]. It is important to note that contribution to the error from cosmic variance is proportional to the underlying theoretical/true C_1^T spectrum. To obtain the total error bars σ_1 used in the IRL deconvolution eq. (2.14), we should add the cosmic variance for the theoretical $C_1^{(i)}$ to the the statistical error bars given with the binned data. However, $C_1^{(i)}$ rapidly iterates to C_1^D within the error bars in the IRL method and the simpler option of using C_1^D instead $C_1^{(i)}$ for computing the cosmic variance works equally well since σ_1 in eq. (2.14) simply regulates the convergence of IRL [58].

We consider a flat Λ -CDM universe, with Hubble constant, $H_0 = 71 \text{ km s}^{-1} \text{ Mpc}^{-1}$; Baryon density, $\Omega_b h_0^2 = 0.0224$, a cosmological constant corresponding to $\Omega_\Lambda = 0.73$, with the remaining balance of matter to critical density in cold dark matter. This is the ‘concordance’ cosmological model suggested by the WMAP parameter estimation. While we mainly focus attention on a cosmological model without early reionization (optical depth to reionization, $\tau = 0$) we do present in section III C the recovered primordial spectra for models with early reionization with opacity going up to $\tau = 0.25$. The case for a large optical depth comes from the temperature-polarization cross correlation. For simplicity, we limit ourselves to the temperature anisotropy spectrum and avoid undue attention to the cosmology suggested by the yet incomplete polarization data. The polarization spectrum is expected to be announced by WMAP soon. It is then easy to extend our method to include both the temperature and polarization anisotropy spectra.

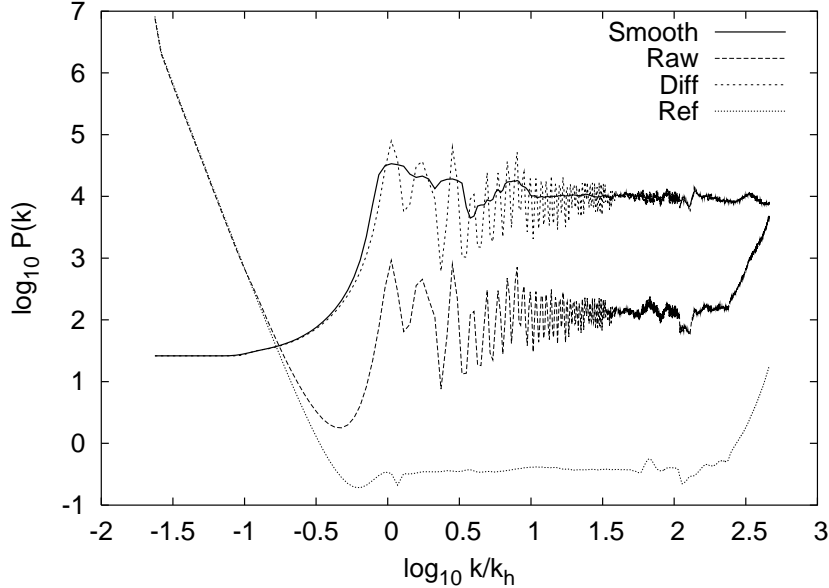


FIG. 3: The three stages leading to the final recovered spectrum for a base cosmological model ($\tau = 0.0$, $h = 0.71$, $\Omega_b h^2 = 0.0224$ and $\Omega_\Lambda = 0.73$) is shown. The lower dashed line is the raw deconvolved power. The upper dashed line is the differenced spectrum obtained by dividing out by the reference spectrum shown as a dotted line. The solid line is the final result after smoothing that gives the best likelihood.

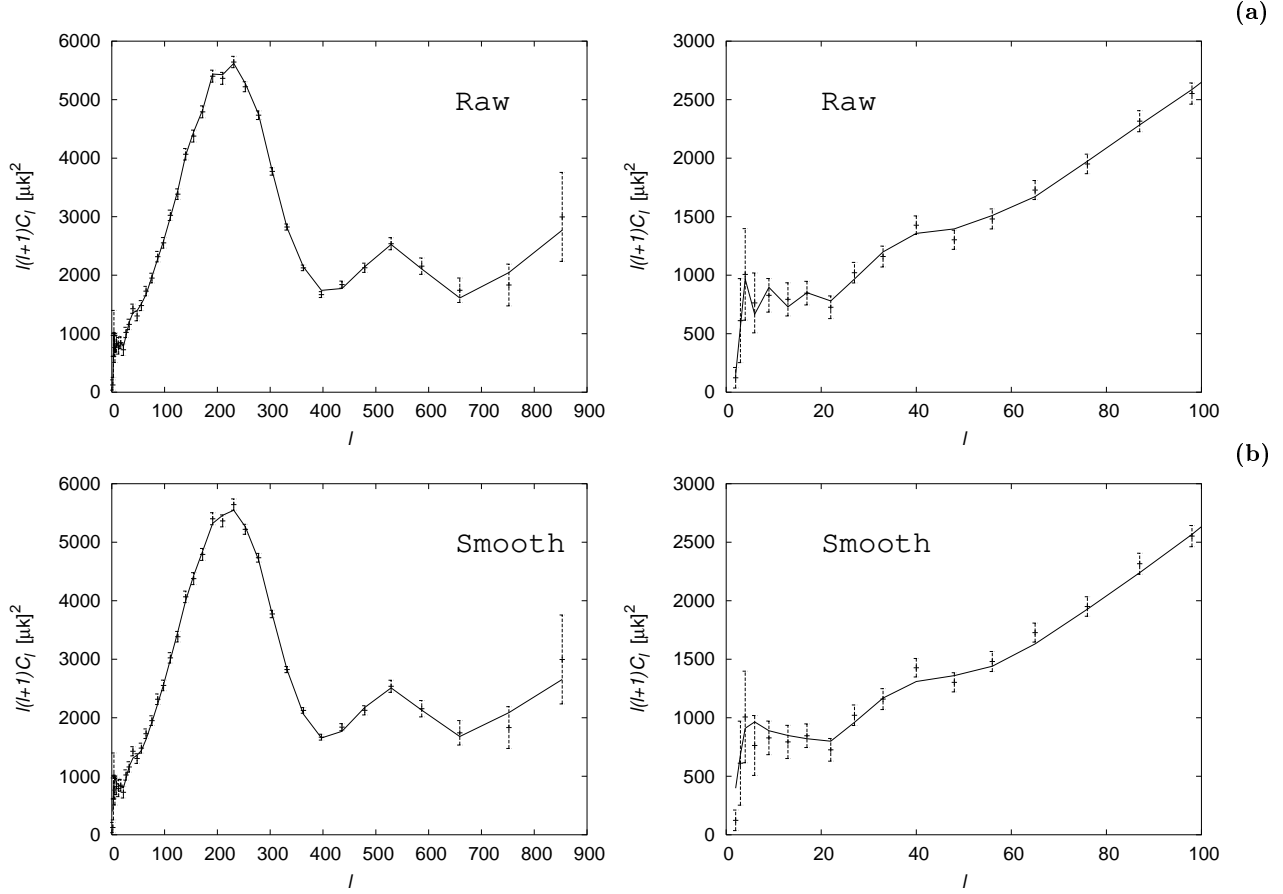


FIG. 4: The recovered C_1 corresponding to the raw $P(k)$ are shown in the upper row and that corresponding to the final smoothed $P(k)$ spectrum are shown in the lower row. The left panels show the full range of multipole, while the right hand panels zoom into the low multipoles. The C_1 's from the raw as well as final $P(k)$ fit the binned C_1^D well ($\chi^2 \approx 10$ and $\chi^2 \approx 20$, respectively for 38 points). However, the jagged form of the C_1 between the 1 bins (apparent in the low multipoles on the right) leads to poor WMAP likelihood for the C_1 from the raw $P(k)$. The differencing and smoothing procedure irons out the jagged C_1 dramatically improving the WMAP likelihood for the final smoothed $P(k)$. The WMAP likelihood is more relevant since it incorporates the estimation of each C_1 and the full error covariance.

B. Primordial power spectrum from WMAP

We apply the method described in the previous section to the WMAP data. Fig. 3 shows the raw deconvolved spectrum, the reference spectrum, the differenced spectrum and the final recovered spectrum after smoothing obtained at each step of our method outlined in section II.

We discuss the advantage of using improved Richardson-Lucy (IRL) in appendix A 2. The effect of IRL method is also evident in Fig. 4. The C_1 from the recovered $P(k)$ matches the binned C_1^D only within the error-bars. The C_1 spectrum corresponding to the differenced and smoothed $P(k)$ is shown in Fig. 4. Although, the former has better χ^2 for the binned data, the WMAP likelihood of the latter is much better. The poor likelihood of the differenced spectrum arises because there is no check on fluctuations in C_1 at intermediate multipoles between the bin centers arising from the spurious numerical effects of k -space and l -space sampling. Better WMAP likelihood is more relevant than good χ^2 for the binned data since the former incorporates the estimation of each C_1 and the full error covariance. Thus the smoothing step our method is carried out with a well defined goal of maximizing the WMAP likelihood.

The primordial spectra recovered from WMAP data is again shown in Fig. 5. The dark solid line is the primordial spectrum that has the best WMAP log-likelihood of $\ln L = -478 \pm 20$ for the base

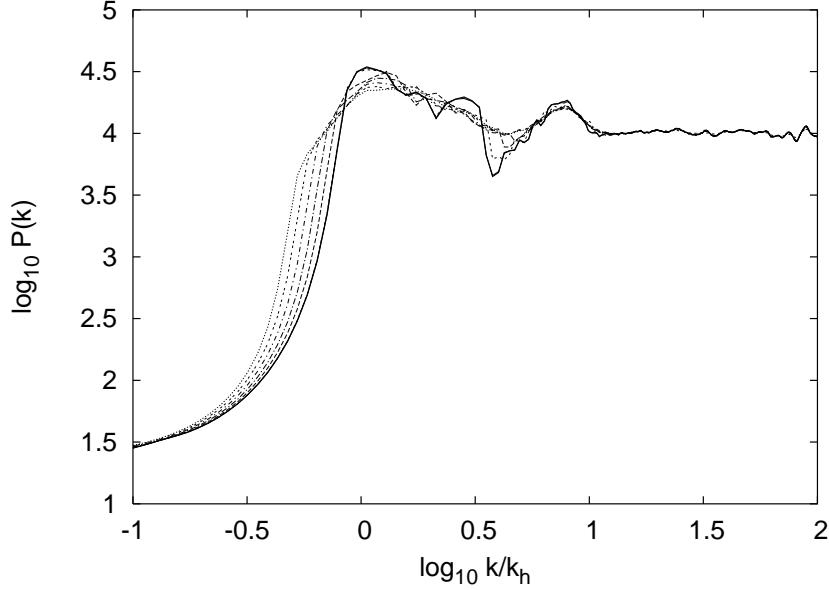


FIG. 5: The final recovered spectrum for the base cosmological model ($\Omega_m = 0.3$, $h = 0.71$, $\Omega_b h^2 = 0.0224$ and $n = 0.95$) is compared with set of $P(k)$ with WMAP likelihood within 2σ . The thick line gives the best likelihood equal to -478.2 and the other lines gives the likelihood bigger than -480 . We can see that the sharp infra-red cut off is common to all these recovered spectra. The infra-red cutoff is remarkably close to the horizon scale and appears to be a robust feature. Another significant and robust feature is the bump just above the cut-off (reminiscent of the oscillation from under-damped transient). The difference between these spectra are in the smoothing and removing the noises from the raw deconvolved spectrum.

cosmological model described in the previous section. The other lines have likelihood $\ln L > -480$, i.e., roughly within 2σ of the best one. For comparison, the same cosmological model with a scale invariant (Harrison-Zeldovich) primordial spectrum has $\ln L = -503.6$, and, with a tilted scale free primordial spectrum $n = 0.95$, the likelihood improves to $\ln L = -489.3$. (A comparison of likelihood numbers for various primordial spectra is given in Table I.) The improvement in likelihood for the recovered spectra is striking.

The most prominent feature of the recovered spectrum is the infra-red cutoff in the power spectrum remarkably close to the horizon scale ($k_c = k_h/2 \approx 0$) chiefly in response to the low quadrupole measured by WMAP. Another notable point is the slight tilt ($n \approx 0.95$) of the plateau in the recovered spectrum at large k which is consistent with the best fit n obtained by WMAP for power law primordial spectra. After the WMAP results, model power spectra with infra-red cutoffs of the form

$$P(k) = A_s k^{1-n_s} \frac{h}{1} e^{-(k/k_c)^{1/2}} \quad (3.2)$$

invoked to explain the suppressed low multipoles of WMAP have had limited success [26, 27]. While the effective $\chi^2_{\text{eff}} = -2 \ln L$ improved by at least 22 over a power law model, the model infra-red cutoff eq. (3.2) could improve the χ^2_{eff} merely by 3 [27]. Figure 6 compares the recovered spectrum with these model infra-red spectra. The power law spectrum shown in the figure also highlights the small tilt ($n \approx 0.95$) recovered by our method.

C. Dependence on the cosmological parameters

The primordial spectrum is recovered for a set of ‘best fit’ cosmological parameters defining the ‘base’ model. We have varied each cosmological parameter by the quoted 1σ error-bars of the WMAP estimates [2]. Figure 7 shows the dependence of the recovered power spectrum on small changes to cosmological parameters varied one at a time keeping the others fixed at their central

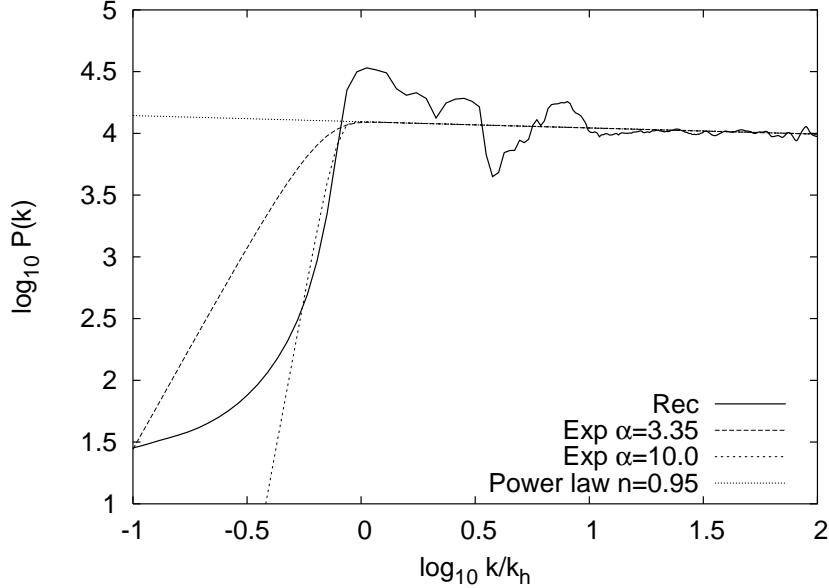


FIG. 6: Comparison between our recovered $P(k)$ and exponential form of infra-red cut off recently studied to explain the suppressed quadrupole of WMAP angular power spectrum [26, 27]. We note that the infra-red cut-off of the recovered spectrum is very steep. The power excess just above the cutoff in the recovered is extremely significant in the remarkably enhanced likelihood. The power spectrum ($n = 0.95$) shows that our method does recover the preferred tilt obtained by WMAP team parameter estimation with power law spectrum [2].

value. We find that recovered spectrum is insensitive to variations Hubble constant, H_0 , modulo an overall shift due to the change in the horizon size, θ_0 . The WMAP likelihood of the corresponding C_1 are $-\ln L = 477.79$ and 478.83 at $h = 0.68$ and 0.75 , respectively. The variation of Baryon density around its middle value $\Omega_B = 0.044$ yields almost identical primordial power spectra with a minor change in likelihood $-\ln L = 477.97$ and 478.53 for $\Omega_B = 0.040$ and $\Omega_B = 0.048$, respectively. The variation of Ω_0 (or equivalently, Ω_m , for flat models) modulo a shift due to change in θ_0 , affects only the amplitude of the infra-red cut-off. The WMAP likelihood of the corresponding C_1 are $-\ln L = 478.93$ and 478.25 for $\Omega_0 = 0.69$ and $\Omega_0 = 0.77$, respectively.

We note that the likelihood at the central values are not necessarily the best. This suggests that, as discussed in the introduction, one should explore the entire space of cosmological parameters and compute the likelihood after optimizing with ‘best’ recovered primordial spectrum. Such an analysis is certainly possible, but has large demands on computational resources. Hence, we defer it to a future publication.

Finally, we also consider the effect of a cosmological model with significant optical depth to reionization, $\tau = 0.17$, such as suggested by the angular power spectrum of the temperature-polarization (TE) cross correlation from WMAP [28]. It has been pointed out that the estimated τ increases when the primordial spectrum has an infra-red cut-off. We compute the primordial power spectrum for base cosmological models with $\tau = 0.10; 0.17; 0.25$. The standard RL deconvolution performs poorly for these models, and, the improved RL method was crucial for these models. Fig. 8 compares the recovered primordial spectra for early reionization models which all show an infra-red cutoff at the horizon scale [59].

IV. THEORETICAL IMPLICATIONS OF THE RECOVERED SPECTRA

The direct recovery of the primordial power spectrum has revealed an infra-red cutoff of a very specific form. Model spectra with monotonic infra-red cutoff such as that in eq. (3.2) do not improve the WMAP likelihood significantly. While, to match the low value of the quadrupole, a very sharp cut-off (such as $\alpha = 10$, see fig 6) is required, such a steep monotonic cut-off tends to pull down the power in the next few higher multipoles above the quadrupole and octopole as well.

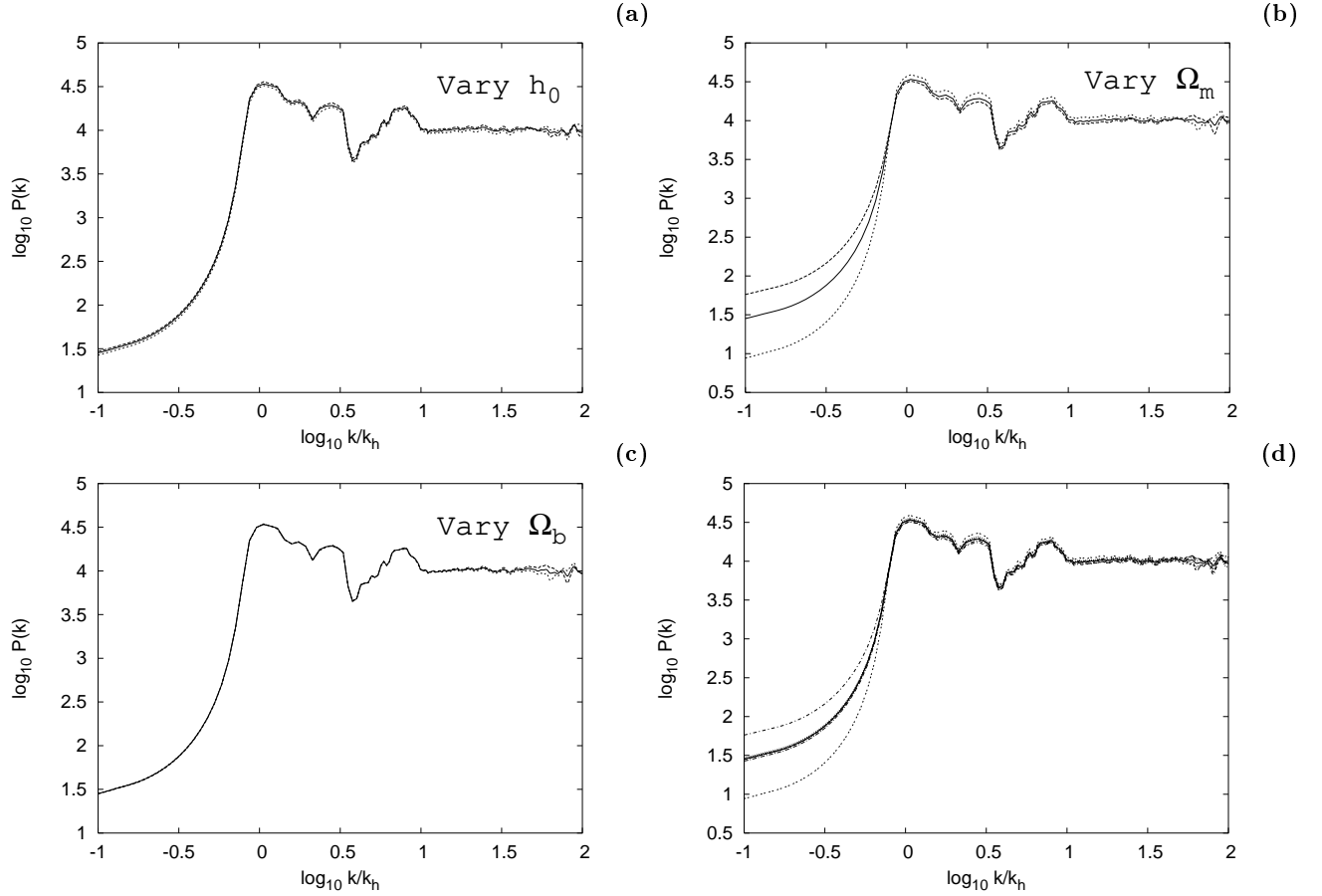


FIG. 7: The panel of figures shows the robustness of the recovered $P(k)$ for variations in the cosmological parameters. Each parameter is varied within the 1σ range indicated by the WMAP parameter estimates [2]. In Fig. (a), the Hubble constant $h_0 = 0.68$, $h_0 = 0.71$ and $h_0 = 0.75$ in the three curves. In Fig. (b) the values of vacuum density $\Omega_m = 0.69$, $\Omega_m = 0.73$ and $\Omega_m = 0.77$ in the three curves. In fig. (c), the Baryonic density $\Omega_b = 0.040$, $\Omega_b = 0.044$ and $\Omega_b = 0.048$ in the three curves. The fig. (d) combines all the distinct curves in other figures to give a consolidated perspective on the dependence of the recovered spectrum on cosmological parameters. Note that the x-axis is the wavenumber is scaled in units of the $k_h = 2 \times 10^0$ which reduces the scatter considerably in the curves for variations in H_0 and Ω_m .

Our recovered spectrum has a compensating excess which allows a steep cut-off to match the low quadrupole and octopole without suppressing the higher multipoles. Naively, one would think that a designer infra-red cutoff would ‘cost’ in the language of Bayesian evidence due to the introduction of extra parameters. That is not necessarily so. An infra-red cut-off of the form we recover does not necessarily have more parameters than an infra-red cut-off of the form in eq. (3.2). Moreover, it is striking that the location of the cut-off is close to a well known scale – the horizon scale.

In this section we show that infra-red cut-off of the form we recover arises from very simple scenarios in inflation. We explicitly mention two of them. Starobinsky [4] has shown that a kink (sharp change in the slope) in the inflaton potential can modulate the underlying primordial power spectrum $P_o(k)$ with a step like feature at a wavenumber k_c

$$\begin{aligned}
 P(k) &= P_o(k) D(k; k_c; r) \\
 &= A_s k^{1-n_s} \left[1 - 3(r-1)^2 \left(\left(1 + \frac{1}{y^2}\right) \sin 2y + \frac{2}{y} \cos 2y \right) \right. \\
 &\quad \left. + \frac{9}{2} (r-1)^2 \frac{1}{y^2} \left(\left(1 + \frac{1}{y^2}\right) \cos 2y - \frac{2}{y} \sin 2y \right) \right]
 \end{aligned} \tag{4.1}$$

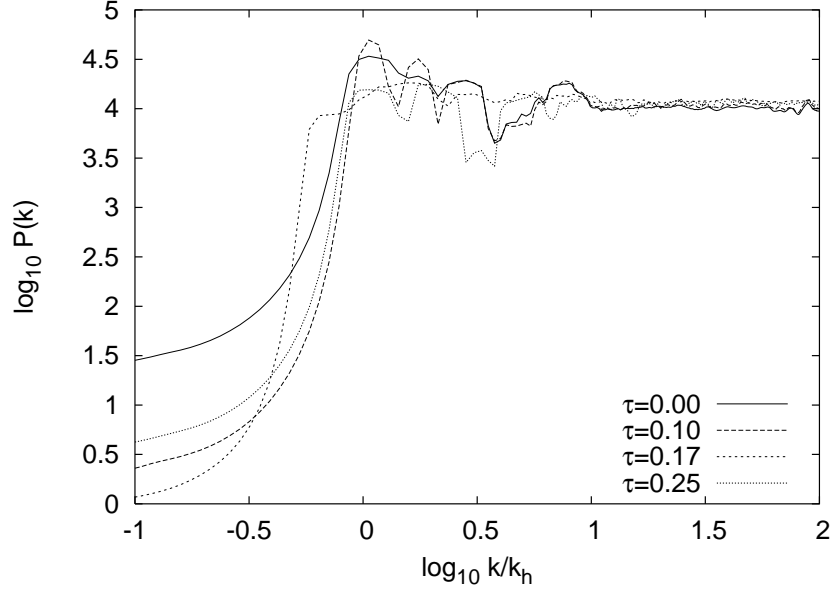


FIG. 8: The recovered $P(k)$ for different values of optical depth ($\tau = 0.00, 0.10, 0.17$ and 0.25). The width of smoothing used is different for different cases. This is the main cause of the small shift in the location of the infra-red cutoff.

where we assume a power law $P_o(k) = A_s k^{1-n_s}$, $y = k/k_c$ and r is the ratio of the slope $dV/d\phi$ before and after kink in the inflaton potential. The power spectrum $P(k)$ in eq. (4.1) has a step up (going to larger k) for $r < 1$ and a step down feature for $r > 1$. An infra-red cut off is created with $r < 1$. Fig. 9 shows a spectrum with a Starobinsky step (eq. 4.1) that can not only mimic the sharp infra-red cutoff but also produces the required bump after it. Table I shows that a introducing an appropriate Starobinsky step gives a very good WMAP likelihood compared to eq. (3.2). Besides the location of the break, k_c , the Starobinsky step spectrum has only another parameter r that fixes the slope and the depth of the cut-off as well as the size of the bump. We have not systematically searched through the (r, k_c) parameter space to arrive at a ‘best-fit’ model. Hence, it may be possible to get even better match to the WMAP data with Starobinsky breaks. Similar scenarios have been studied earlier [29] and has also been pointed to in the post-WMAP literature [30]. Multiple scalar field inflation provide ample scope for generating features in the primordial spectrum [3] and has been invoked to model a sharp cut-off at horizon scale (see eg., [31, 32]). More exotic origin of an infra-red cut off in the scalar spectrum have also been investigated [33, 34, 35, 36, 37].

Another compelling theoretical scenario for generating a feature of the form we have recovered is well-known. It is well known that radiation, or matter dominated era prior to inflation does affect the primordial power spectrum on scales that ‘exit the horizon’ soon after the onset of inflation. For a pre-inflationary radiation dominated epoch the power spectrum was given by Vilenkin and Ford (VF) [5]

$$P(k) = A_s k^{1-n_s} \frac{1}{4y^4} e^{2iy} (1 + 2iy)^{-1} \frac{2y^2}{y^2} \quad (4.2)$$

where $y = k/k_c$. Fig. 9 shows that the VF spectrum (eq. 4.2) can also provide an infra-red cutoff with required bump after it. Table I shows that a VF spectrum can give better WMAP likelihood compared to model spectra of the form eq. (3.2). The infra-red cut-off ($\propto k^2$) here is not very sharp. However, if the epoch prior to inflation is dominated by matter with some other equation of state, the slope would be different. A more complete analysis may give rise to spectra closer to the kind we have recovered. The scale k_c is set by the Hubble parameter at the onset of inflation. For this scenario to be applicable to our results, the k_h -mode corresponding to the horizon scale must have crossed the Hubble radius very close to the onset of inflation. In a single scalar field inflation this would happen naturally [38].

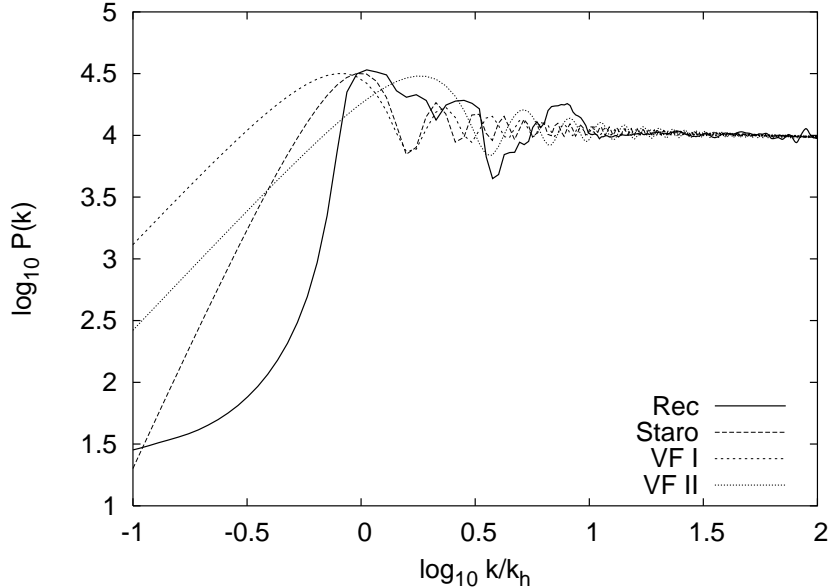


FIG. 9: Comparison of our recovered $P(k)$ (solid) with the predictions two simple theoretical scenarios that remarkably match the gross features of the infra-red cutoff in the recovered spectrum. The ‘staro’ curve is the primordial spectrum when the inflaton potential has a kink– a sharp, but rounded, change in slope [4]. Fine tuning is involved in locating the kink appropriately. The ‘VF’ curves are the modification to the power spectrum from a pre-inflationary (here, radiation dominated) epoch [5]. This requires that the horizon scale, k_h , exits the Hubble radius very soon after the onset of inflation. Although, it appears fine tuned there is corroborating support for this within single scalar field driven inflation [38]. The theoretical $P(k)$ leads to C_1 that enhanced WMAP likelihood given in Table I. The values of the parameters for the theoretical curves are given in the same table.

Another possibility is that the infra-red cutoff arises due to non-trivial topology of the universe. A dodecahedral universe model that matches the low multipoles of WMAP angular spectrum has been proposed [39]. In future work we would like to check whether the recovery of a discrete initial spectrum with our method appears similar to the spectrum we recovered here. However, non-trivial cosmic topology is expected to also violate the statistical isotropy of the CMB anisotropy and give rise of correlation features which are potentially detectable [40].

V. DISCUSSION AND CONCLUSIONS

The CMB anisotropy is usually expected to be statistically isotropic and Gaussian [41]. In that case, the angular power spectrum of CMB anisotropy encodes all the information that may be obtained from the primary CMB anisotropy, in particular, the estimation of cosmological parameters. It is very important to note that cosmological parameters estimated from CMB anisotropy (and other similar observations of the perturbed universe) usually assume a simple parametric form of spectrum of primordial perturbations. It is clear, however, that estimation of cosmological parameters depends on the extent and nature of parameterization of the primordial (initial) perturbations included into the parameter space considered [6].

We proceed on a complimentary path of determining the primordial power spectrum directly from the CMB anisotropy for a set of cosmological parameters. Assuming the best fit cosmological parameters from WMAP, our method applied to the angular power spectrum measured by WMAP yields interesting deviations from scale invariance in the recovered primordial power spectrum. The recovered spectrum shows an infrared cut-off that is robust to small changes in the assumed cosmological parameters. The recovered spectrum points to the form of infra-red cut off that matches the low multipoles of WMAP. We also show that the such forms of infra-red cut-off can arise from simple well-known effects with inflation. It is important to recall that the angular power spectrum from the ‘full’ sky CMB anisotropy measurement by COBE-DMR [42] also indicated an

TABLE I: The effective chi-square, $\chi^2_{\text{eff}} = 2 \ln L$, of the C_l corresponding our recovered spectrum is compared with a number of model primordial spectrum (with or without the infra-red cutoff. Limited attempt has been made to search for the best parameter values and the χ^2_{eff} for the model spectra should be treated as indicative and are strictly upper bounds.

Power spectrum	χ^2_{eff}	$2 \ln L$	$k_c = k_h^a$ ($k_h = 4.5 \cdot 10^{-4} \text{ Mpc}^{-1}$)
Direct Recovered	956.76		0.71
Flat Harrison Zeldovich	1007.28		–
Power Law ($n_s = 0.95$)	978.60		–
Exponential cutoff ($n_s = 0.95, \alpha = 3.35$)	978.08		0.64
Exponential cutoff ($n_s = 0.95, \alpha = 10$)	977.84		0.64
Starobinsky break ($n_s = 0.95, r = 0.01$)	973.86		0.32
Vilenkin & Ford (VF-I) ($n_s = 0.95$)	976.88		0.43
Vilenkin & Ford (VF-II) ($n_s = 0.95$)	978.66		0.96

^aInterpretation of k_c depends on the form of model power spectrum. For the recovered spectrum a simple tangent hyperbolic fit was used.

infra-red cutoff [43]. Although we mostly emphasize the infrared cutoff, the final recovered spectrum shows a damped oscillatory feature after the infra-red break (‘ringing’). It has been pointed out recently that such oscillations improve χ^2_{eff} and could be possibly a signature of trans-Planckian effects [12, 44]. We have not assessed the significance and robustness of the features at large $k=k_h$ that may be consistent with features deduced in the analysis of recent redshift surveys [45].

Here we have considered a ‘best fit’ cosmology and some finite number of variations around it [60]. However, with large but reasonable computational resource, it is possible to explore a multi-dimensional space of cosmological parameters to compute a likelihood at each point for an optimal (recovered) primordial spectrum.

In this work, we have used only the angular power spectrum of WMAP measured temperature fluctuations (TT). Once the E-polarization power spectrum (EE) is announced by the WMAP team, our method can be extended to include TE and EE angular power spectra in obtaining the primordial power spectrum. It is also possible extend our recovery of the primordial spectrum to larger wave-numbers by using the matter density power spectrum measured by large scale redshift surveys such as the Sloan Digital sky survey SDSS and 2degree Field survey, measurement from Ly- α absorption, and possibly, weak gravitational lensing in the near future [49, 50].

In the absence of a definitive and precise scenario for the generation of primordial perturbations, a direct inversion of the primordial spectrum is an extremely appealing approach made possible by the remarkable quality of the recent cosmological data, in particular, the anisotropy in the cosmic microwave background temperature.

Acknowledgments

We greatly benefited from the exploratory attempt to solve the problem using a non-iterative method by V. Gopisankararao as part of the visiting student programme at IUCAA in the summer of 2001. We acknowledge very useful discussions with S. Sridhar and N. Sambhus regarding the RL deconvolution method. AS thanks IUCAA for use of its facilities during his Master thesis work.

APPENDIX A: SOME ASPECTS OF THE METHOD.

In this appendix, we provide support and justification for some steps in our method for recovering the primordial power spectrum. In section A 1 we demonstrate the robustness of the iterative Richardson-Lucy deconvolution to changes in the initial guess. The next section (A 2) discusses the advantage of the improved Richardson-Lucy method used in our work. In the last section (A 3), we model the broad features of reference spectrum analytically and show that it is well understood.

1. Effect of the initial guess in the Richardson-Lucy method

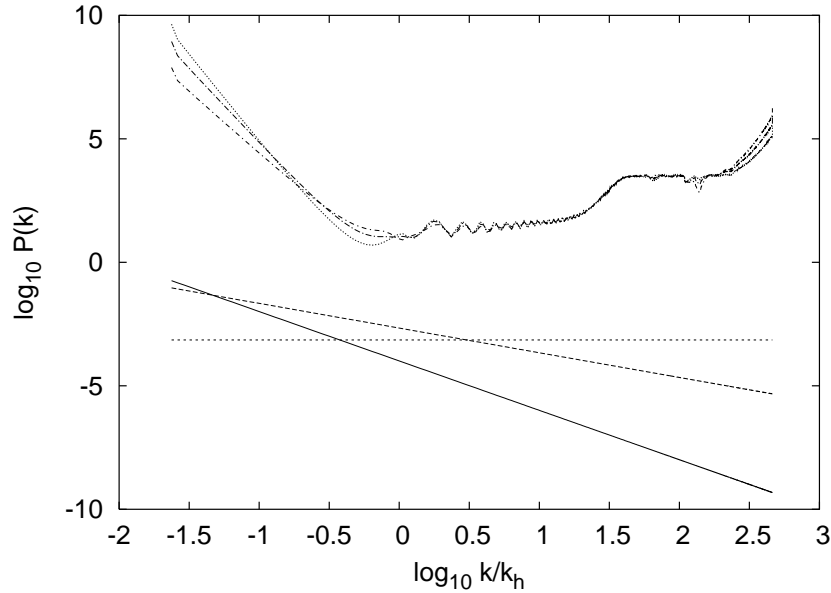


FIG. 10: The figure shows the raw power spectrum recovered using the Richardson-Lucy algorithm starting from three different initial guesses. The effect of the initial guess is negligible in the other region k space. As shown in the next section A 3, the artefacts at low k and high k which are removed by the reference spectrum have a known dependence on the initial guess.

The effect of the initial guess is negligible in the Richardson-Lucy method of deconvolution for our problem. We find that the result for various different initial guesses come very close to each other after a few iterations. Here we demonstrate the robustness of our method by deconvolving using the C_1 from a test spectrum (with a step) using different initial guesses. In Fig. 10 deconvolved raw $P(k)$ arising from different forms of the initial guess spectra

$$P(k) = \text{constant}; \quad P(k) = 1/k; \quad P(k) = 1/k^2; \quad (\text{A1})$$

are shown. The effect of the initial guess is absent in the portion of the k space probed well by the kernel. The deconvolved spectra are almost identical for all these different initial guesses in that region of k space. As discussed in section A 3, the dependence of deconvolved spectrum at the small and large k ends is well understood and get largely removed when divided by the reference spectrum. In a previous work we have checked a large variety of initial guesses and concluded the RL method applied to our problem of recovering the primordial spectrum from the CMB anisotropy is independent of the initial guess. [7].

2. The Improved Richardson Lucy method

In this section we show the advantage of the improved Richardson Lucy algorithm given by eq. (2.14) over the standard method given by eq. (2.13). We compare the raw power spectrum

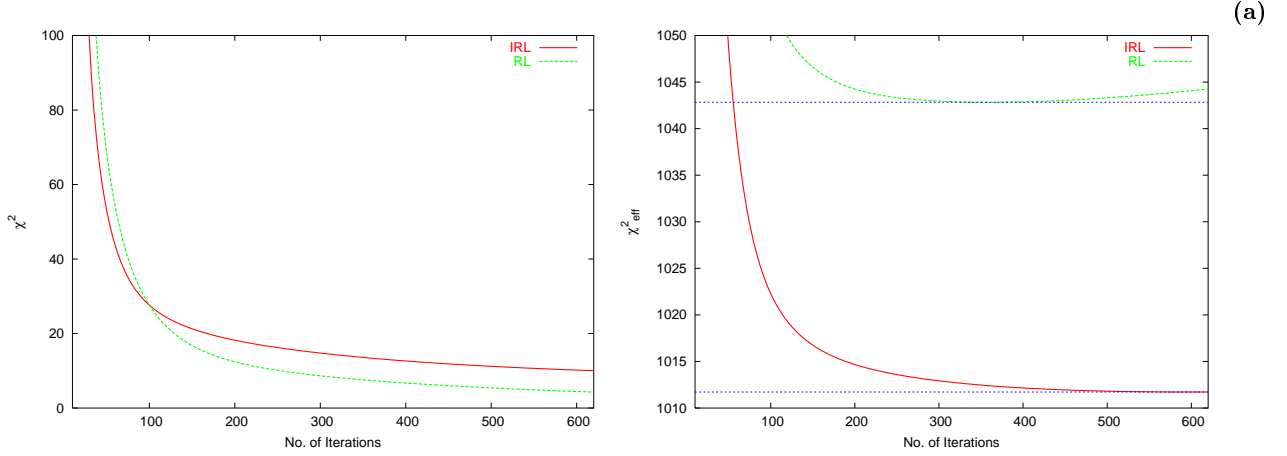


FIG. 11: The left panel plots the variation of χ^2 of $C_1^{(i)}$ obtained after i th iteration (w.r.t the binned WMAP spectrum, C_1^D) with increasing iterations for the Richardson-Lucy (RL) method and improved version (IRL) we present in this work. The panel on the right, plots the variation of $\chi^2_{\text{eff}} = \chi^2 / 2 \ln L$ of the $C_1^{(i)}$ given by the WMAP likelihood, L . In contrast to RL, in the IRL method χ^2_{eff} converges with iteration and to a significantly lower value.

$P^{(i)}(k)$ and the corresponding angular spectrum $C_1^{(i)}$ obtained from the WMAP binned angular power spectrum, C_1^D using RL and IRL algorithm as the iterations progress. In Fig. 11, the left panel shows the χ^2 of $C_1^{(i)}$ w.r.t C_1^D . As expected, the RL method leads to a lower (better) χ^2 than the IRL method. However, we are interested in recovering a $P(k)$ which give C_1 that has better likelihood with respect to WMAP data. The right panel of Fig. 11 plots the WMAP likelihood given in terms of $\chi^2_{\text{eff}} = \chi^2 / 2 \ln L$. This figure justifies the ‘improved’ label to the IRL method. For the RL case, the value of χ^2_{eff} is seen to bounce and increase at large iterations. (This bounce is more pronounced and happens at a lower iteration for certain cosmological model, e.g., one with high optical depth to reionization, $\tau_{\text{re}} \approx 0.1$.) This is a reflection of the problem of the RL method fitting the noise in the data. In contrast, in the IRL case the χ^2_{eff} converges with iterations and to significantly better (lower) value than that for the RL case.

3. Reference spectrum

In this subsection, we show that the reference spectrum used to remove numerical artifacts from the raw power spectrum recovered by the deconvolution is analytically well understood. The reference spectrum reflects the sensitivity of the kernel $j(l; k)j^2$ to the k space. (Here, the overbar in $j(l; k)j^2$ alludes to the binned version related to $G(l; k)$ following eq. (2.7)). In the regions of k space where the kernel probes $P(k)$ weakly, there is scope for changing the power spectrum without changing the C_1 . In such degenerate regions, the Richardson Lucy method (both RL and IRL) pushes the power spectrum up to the extent possible changing the C_1 .

Fig. 12 shows that the strong features at the low k and high k are well fitted by analytically obtained power law forms. At the low wavenumbers ($k=k_{\text{h}}-1$), the CMB anisotropy is dominated by the Sachs-Wolfe effect. The sensitivity of the CMB anisotropy to the power at very small wavenumbers is dominated by the lowest multipole as $j(l; k)j^2 \propto k^{2l}$. This is the well known Grishchuk-Zeldovich effect [51]. When the quadrupole is included, $j(l; k)j^2 \propto k^4$ is the strongest probe of the $P(k)$ at low wavenumbers. Hence, there is no change to C_1 (here, chiefly the quadrupole) caused from this region of k space from the initial guess $P^{(0)}(k)$ onward if $P(k) \propto k^{4+\epsilon} P^{(0)}(k)$ for $\epsilon > 0$. In our work we have used an initial guess of the form $P^{(0)}(k) \propto 1/k^2$. Hence, the slope of $P(k)$ at low k is driven to the k^{-6} form shown in Fig. 12.

At the large k end, the $j(l; k)j^2$ is governed by the power slope of the tail in the sensitivity of the highest few multipole bins shown plotted in Fig. 12. The slope of these tails are well fitted by a power law form $k^{-7/2}$. Using the same argument, it is clear that there will be no change to the

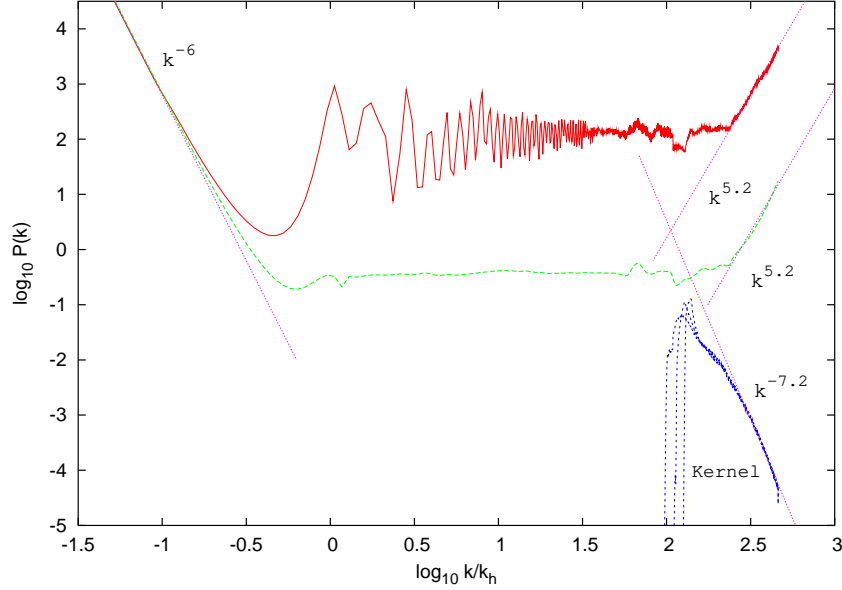


FIG. 12: The figure shows the $P_{\text{raw}}(k)$ and $P_{\text{ref}}(k)$ obtained from the WMAP binned data C_1^D for an initial guess $P^{(0)}(k) / 1=k^2$. The dashed straight line labeled corresponds to the analytical power law form $(k^{-4}P^{(0)}(k) = k^{-6})$ that matches the identical fall in $P_{\text{raw}}(k)$ and $P_{\text{ref}}(k)$ at low k . The dashed line matching the rise in $P_{\text{raw}}(k)$ and $P_{\text{ref}}(k)$ at large k corresponds to the analytical power law form $(k^{7/2}P^{(0)}(k) = k^{5/2})$ expected from the roughly $k^{-7/2}$ tail of the kernels for the last few multipole bins.

C_1 caused from this region of k space from the initial guess onward if $P(k) / 1=k^{7/2} P^{(0)}(k)$. For the initial guess $P^{(0)}(k) / 1=k^2$, the rise at high k end is driven to a $k^{5/2}$ form.

The division of reference spectrum used here is a simple numerical recipe for estimating and removing the artefacts of the deconvolution method for a given kernel. We have shown that the gross features of the $P_{\text{ref}}(k)$ can be understood analytically. The finer features of $P_{\text{ref}}(k)$ are likely linked to the details of the structure of $j(k)j^2$ and will be explored in future work.

-
- [1] C. L. Bennett et al., *Astrophys.J.Suppl.* **148**, 1, (2003).
 - [2] D. N. Spergel et al., *Astrophys.J.Suppl.* **148**, 175, (2003).
 - [3] A. A. Starobinsky, *Pisma Zh. Eksp. Teor. Fiz.* **42**, 124 (1985) [*JETP Lett.* **42**, 152 (1985)]; L. A. Kofmann, A. D. Linde and A. A. Starobinsky, *Phys. Lett.* **B157**, 361 (1985); L. A. Kofmann and A. D. Linde, *Nucl. Phys.* **B 282**, 555 (1987); J. Silk and M. S. Turner, *Phys. Rev.* **D 35**, 419 (1987); L. A. Kofmann and D. Y. Pogosyan, *Phys. Lett.* **B214**, 508 (1988); J. R. Bond and D. Salopek, *Phys. Rev.* **D 40**, 1753, (1989); H. M. Hodges, G. R. Blumenthal, L. Kofman, J. Primack, *Nucl.Phys.* **B335**, (1990); V.F. Mukhanov and M.I. Zelnikov, *Phys.Lett.* **B263**, 169,1991; D. Polarski and A. A. Starobinsky, *Nucl. Phys.* **B385**, 623 (1992); J. Lesgourgues, D. Polarski and A. A. Starobinsky, *Mon. Not. R. Astron. Soc.* **308**, 281 (1999); J. Lesgourgues, S. Prunet and D. Polarski, *Mon. Not. R. Astron. Soc.* **303**, 45 (1999).
 - [4] A. A. Starobinsky, *JETP lett.* **55**, 489 (1992).
 - [5] A. Vilenkin and L. H. Ford, *Phys.Rev.* **D26** 1231 (1982).
 - [6] T. Souradeep, J. R. Bond, L. Knox, G. Efstathiou and M.S. Turner, *Proc. COSMO-97 – International workshop on ‘Particle Physics and Early Universe’ Sept. 15-19, 1997, Ambleside, U.K.*, (ed L. Roszkowski, World Scientific, 1998), astro-ph/9802262.
 - [7] A. Shafieloo, *M. Sc. dissertation*, Supervisor T. Souradeep, Univ. of Pune, (2002).
 - [8] S. L. Bridle, A. M. Lewis, J. Weller, G. Efstathiou, *Mon. Not. Roy.Astron. Soc.* **342** L72 (2003).
 - [9] P. Mukherjee and Y. Wang, *Astrophys. J.* **598** 779 (2003).
 - [10] S. Hannestad, *JCAP*, **0404**, 002 (2004)
 - [11] M. Matsumiya, M. Sasaki, J. Yokoyama, *Phys.Rev.* **D65**, 083007, (2002); *ibid*, *JCAP* **0302** 003 (2003).
 - [12] N. Kogo, M. Matsumiya, M. Sasaki, J. Yokoyama *Astrophys.J.* **607** 32 (2004).
 - [13] A. Niarchou, A. H. Jaffe and L. Pogosian, *Phys.Rev.* **D69** 063515 (2004)

- [14] U. Seljak and M. Zaldarriaga, *Astrophys.J.* **469**, 437 (1996). (<http://cmbfast.org/>).
- [15] S. Podariu, T. Souradeep, J. R. Gott III, B. Ratra and M. S. Vogeley, *Astrophys. J.*, **559**, 9, (2001).
- [16] L. B. Lucy, *Astron. J.*, **79**, 6 (1974).
- [17] B. H. Richardson, *J. Opt. Soc. Am.*, **62**, 55, (1972).
- [18] C. M. Baugh and G. Efstathiou, *Mon.Not.Roy.Astron.Soc.* **265**, 145 (1993).
- [19] C. M. Baugh and G. Efstathiou, *Mon.Not.Roy.Astron.Soc.* **267**, 323 (1994).
- [20] R. L. White, A. S. P. Conference series, **61**, 292 (1994).
- [21] G. Hinshaw, et.al., *Astrophys. J. Suppl.*, **148**, 135 (2003).
- [22] M. Limon, et.al., *First Year Wilkinson Microwave Anisotropy Probe (WMAP) Observations: Explanatory Supplement* (<http://lambda.gsfc.nasa.gov/>).
- [23] M. Tegmark, A. de Oliveira-Costa, & A. Hamilton, *Phys. Rev.* **D68** 123523, (2003).
- [24] G. Efstathiou, *Mon. Not. Roy. Astron. Soc.* **348**, 885 (2004).
- [25] L. Knox, *Phys.Rev.* **D52**, 4307, (1995).
- [26] C. R. Contaldi, M. Peloso, L. Kofman and A. Linde, *JCAP* **0307**, 002, (2003).
- [27] J. M. Cline, P. Crotty, J. Lesgourgues, *JCAP* **0309** 010 (2003).
- [28] A. Kogut, et.al., *Astrophys.J.Suppl.*, **148**, 161 (2003).
- [29] S. M Leach, M. Sasaki, D. Wands and A. Liddle, *Phys.Rev.* **D64**, 023512, (2001).
- [30] N. Kaloper and M. Kaplinghat, *Phys.Rev.* **D 68**, 123522, (2003).
- [31] J. Yokoyama, *Phys.Rev.* **D 59**, 107303, (1999).
- [32] B. Feng and X. Zhang, *Phys.Lett.* **B570**, 145, (2003).
- [33] S. Tsujikawa, R. Maartens, R. Brandenberger, *Phys.Lett.* **B574**, 141, (2003).
- [34] S. Tsujikawa, P. Singh, R. Maartens, *preprint*, astro-ph/0311015.
- [35] M. Fukuma, Y. Kono, A. Miwa, *preprint*, hep-th/0312298.
- [36] Y. Piao, B. Feng, X. Zhang, *Phys. Rev.* **D63**, 084520, (2000).
- [37] Y. Piao, S. Tsujikawa, X. Zhang, *preprint*, hep-th/0312139.
- [38] J. Lasue and T. Souradeep, *in preparation*.
- [39] J.-P. Luminet et al., *Nature* **425**, 593 (2003).
- [40] A. Hajian and T. Souradeep, *Astrophys. J. Lett.* **597**, L5, (2003); A. Hajian and T. Souradeep, *preprint* (astro-ph/0301590).
- [41] D. Munshi, T. Souradeep and A. A. Starobinsky, *Astrophys.J.* **454**, 552 (1995); D. N. Spergel and D. M. Goldberg *Phys.Rev. D* **59** 103001 (1999).
- [42] G. F. Smoot et al., *Astrophys. J.* **396**, L1, (1992).
- [43] Y. Jing and L. Fang, *Phys. Rev. Lett.* **73**, 1882 (1994).
- [44] J. Martin and C. Ringeval, *Phys.Rev.* **D69**, 083515 (2004).
- [45] D. Tocchini-Valentini, M. Douspis, J. Silk, *preprint*, astro-ph/0402583.
- [46] B. Ratra and J. Peebles, *Phys. Rev. D* **52**, 1837, 1995; K. Yamamoto, M. Sasaki, T. Tanaka, *Phys. Rev. D* **54**, 1996; A. A. Starobinsky, *Proc. of Cosmo-94*, Ed. M.Y. Klopov, M. E. Prokhorov, A. A. Starobinsky, and J. Tran Thanh Van, (Editions Frontieres, 1996); J. R. Bond, D. Pogosyan, and T. Souradeep, *Phys. Rev. D* **62**, 043005 (2000).
- [47] A. A. Starobinsky, *Sov. Astron. Lett.* **11**, 133, (1985); R. Davis et al., *Phys. Rev. Lett.* **69**, 1856, (1992); T. Souradeep and V. Sahni, *Mod. Phys. Lett. A*, **7**, 3541, (1992); R. Crittenden et al., *Phys. Rev. Lett.*, **71**, 324, (1993).
- [48] G. Efstathiou and J. R. Bond, *Mon. Not. R. Astron. Soc.*, **218**, 103, (1986); P. Crotty et al., *Phys. Rev. Lett.* **91**, 171301, (2003); M. Bucher et al., *preprint*, astro-ph/0401417.
- [49] M. Tegmark and M. Zaldarriaga, *Phys. Rev.* **D66**, 103508, (2002).
- [50] E. Gawiser, Ph.D. Thesis, U.C. Berkeley, (1999).
- [51] L. P. Grishchuk and Ya. B Zeldovich, *Soviet Astronomy*, **22**, 125, (1978) [*Astronomicheskii Zhurnal*, **55**, 209, (1978)].
- [52] Estimate of the power spectrum in k space ‘bins’ carried out with recent data is a somewhat model independent [8, 9, 10]. Direct deconvolution with different method [11] has been attempted [12]
- [53] It is possible that very unlikely cosmological parameters get picked out due to suitably tailored initial power spectrum. In this case, one can employ appropriately strong priors from other observation or beliefs to ensure that unlikely, unphysical, ill-motivated are down weighted.
- [54] Binned C_1^D data that combined the heterogeneous CMB band power obtained from different experimental data sets are not always as reliable due to relative calibration uncertainties. Application of our method to binned data of [15] did not give robust or convincing results [7]. However, in principle nothing rules out using binned data from heterogeneous data sets that have good cross-calibration.
- [55] In what follows we assume that the quantities are normalized and omit the overhead tilde in the notation. The normalization to unity not required and it is possible to use other normalizations, such as, $(2l+1)C_1 = \text{constant}$
- [56] The C_1 are uncorrelated for an ideal full-sky map, but in practice, the covariances between neighboring multipole arise due to non-uniform/incomplete sky coverage, beam non-circularity, etc..
- [57] Legacy Archive of Microwave Background Data – <http://lambda.gsfc.nasa.gov/>
- [58] The contribution to the error from cosmic variance given in the WMAP binned power data is computed

using the C_1^T for the best fit Λ -CDM model with a power law primordial spectrum. Our error bars are computed using C_1^D .

- [59] For simplicity and consistency, we use the same smoothing for these cases. Better result can be obtained for $\alpha = 0.17$ with different smoothing.
- [60] Our analysis here is limited to flat models cosmological models. We have also ignored the contribution from tensor perturbations and assumed adiabatic perturbations in this exploratory paper. Although, inflation generically predicts a geometrically flat universe, the power spectrum of perturbations in non-flat universe models has been studied [46]. The effect of tensor perturbations on the CMB anisotropy spectrum is well studied [47] and so is the role of isocurvature perturbations [48]. Hence, it is straightforward to remove these limitations in a more comprehensive future analysis.